Collisional energy transfer between excited Sr atoms

H. G. C. Werij,* M. Harris,† J. Cooper,‡ and A. Gallagher§
Joint Institute for Laboratory Astrophysics, University of Colorado and National Institute of Standards and Technology, Boulder, Colorado 80309-0440

J. F. Kelly
Department of Physics, University of Idaho, Moscow, Idaho 83843
(Received 9 April 1990)

The following energy-transfer reactions have been observed in a Sr vapor following pulsed excitation of the $5\,^1P_1$ state: $Sr^*(5\,^1P_1)+Sr^*(5\,^1P_1)\rightarrow Sr(5\,^1S_0)+Sr^{**}(n^{2S+1}L)-\Delta E$, $Sr^*(4\,^1D_2)+Sr^*(4\,^1D_2)\rightarrow Sr(5\,^1S_0)+Sr^{**}(n^{2S+1}L)-\Delta E$. The $4\,^1D_2$ state was populated by a nonlinear stimulated process. By measuring the rate coefficients for these reactions for over 40 final states $n^{2S+1}L$, we look for insight into how these reactions depend on energy defect, spin, and angular momentum. It is found that there is not a very strong dependence on the energy defect, and that singlet and triplet final states are produced in comparable amounts. The final states tend to be populated more effectively as their angular momentum increases. Total rate coefficients are of the order of gas-kinetic rates.

I. INTRODUCTION

The electronic energy-transfer process[1] in which two excited atoms (A^*) collide to produce one highly excited atom (A^{**}) and one ground-state atom (A) is generally referred to as energy pooling (EP). EP was first reported by Allegrini *et al.*[2,3] for collisions between two Na $3P$ atoms (Na*). Subsequent studies of this system have measured excitation transfer rate coefficients from Na*+Na* to all Na** states within $\sim 1000\ cm^{-1}$ of the initial $3P+3P$ energy,[4–6] as well as to $Na_2^+ + e^-$. In addition, dependences on collision energy and electronic-state alignment have been measured.[7,8] EP rate coefficients involving other atoms have been reported for collisions between pairs of $Sr(5\,^3P_{0,1,2})$ atoms[9] and for heteronuclear systems Na*-K*, Na*+Rb,* and K*+Rb*.[10,11]

In this paper we greatly extend the number of measured EP rate coefficients by studying the following processes:

$$Sr^*(5\,^1P_1)+Sr^*(5\,^1P_1)\xrightarrow{k_{PP}}Sr(5\,^1S_0)+Sr^{**}(n^{2S+1}L)-\Delta E\ ,$$

$$Sr^*(4\,^1D_2)+Sr^*(4\,^1D_2)\xrightarrow{k_{DD}}Sr(5\,^1S_0)+Sr^{**}(n^{2S+1}L)-\Delta E\ .$$

The relevant Sr and Sr-pair energy levels are shown in Fig. 1. In contrast to earlier EP experiments where only a very limited number of final states were observed, here over 40 final states are observed from two different Sr* initial-state pairs.

Energy pooling, or $A^*+A^*\rightarrow A^{**}+A$, collisions initially appear different from the more traditional $A_i^*+B\rightarrow A_j^*+B$ "excitation-transfer" collisions in which B is typically an "inert" gas. However, when a molecular-state picture is used, it becomes apparent that both processes are equivalent, are described by the same formalism, and should show the same general characteristics. To demonstrate this, the general case of electronic energy transfer, $A_i+B_k\rightarrow A_j+B_l$, is shown diagrammatically in Fig. 2. Here the atoms approach (ar-

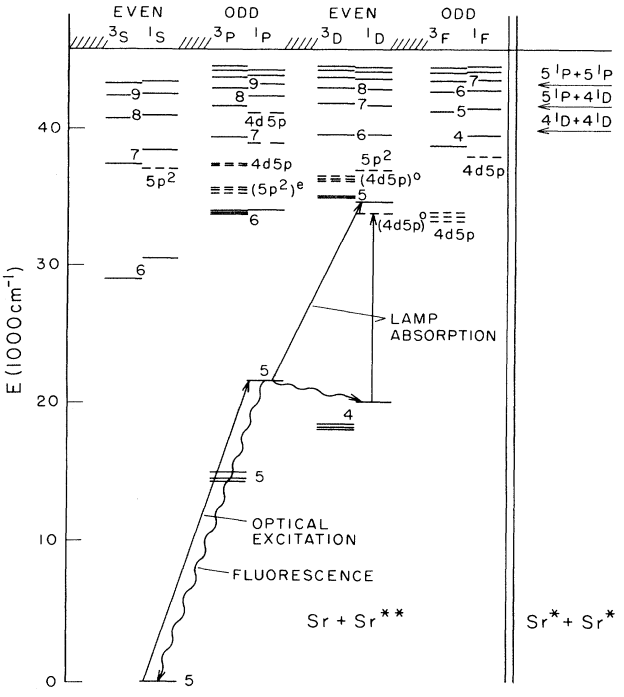

FIG. 1. Sr energy-level diagram, also showing the pair energies of the $5\,^1P$ and $4\,^1D$ states.

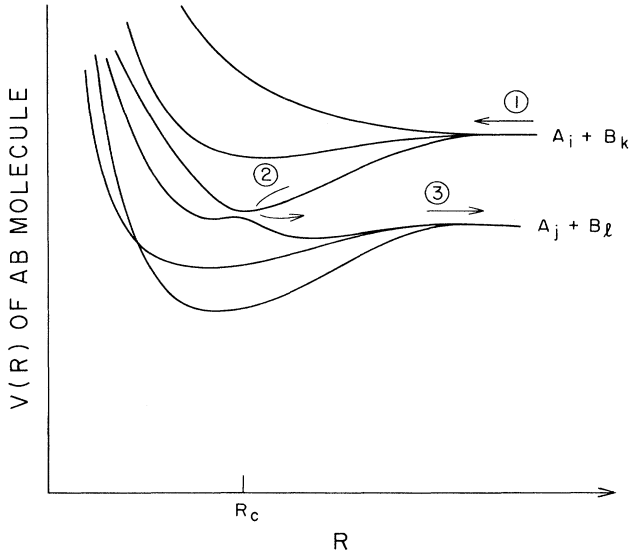

FIG. 2. Diagrammatic representation of electronic energy transfer between atoms A and B initially in electronic states A_i and B_k, where $V(R)$ are adiabatic potential energies of the AB molecules.

row labeled 1) in electronic states A_i and B_k, which are the separated-atom limit of three molecular adiabatic states whose electronic energies $V(R)$ are shown. They branch, with statistical probability, into one of these initial molecular states. Due to the finite speed of internuclear motion, the transient molecule may undergo electronic state change during traversal of the small-R region; the avoided crossing identified by arrow 2 is often the dominant cause of this. When this state change transfers population to one of the lower three states in Fig. 2, the pair separates as A_j+B_l, the separated-atom limit of these three adiabatic states (arrow 3). In the EP case $A_i=B_k$, and A_j is a ground-state atom, while in excitation transfer $B_k=B_l=B$.

Due to this equivalence of EP and normal electronic energy transfer, the present study of EP from two different initial states to ~40 final states is a search for propensities in all electronic energy transfer. From this large array of states we have been able to investigate dependences on energy defects, angular momentum, and spin changes.

II. EXPERIMENT

As is typical for an energy-transfer experiment, we measure the ratio of the final- to initial-state fluorescence intensities. However, as both collision partners are excited in the EP case, one cannot measure the perturber density with a pressure gauge. Densities of the initial collision partners are determined here by their absorption of narrow lines from a Sr hollow-cathode lamp.[9,12–14] For the present study we carefully determined the absolute rate coefficients k_{PP} and k_{DD} for one particular Sr** level, and then measured the other rate coefficients relative to those. The absolute rate coefficients are determined as follows.

In the case of $5\,^1P+5\,^1P$ energy pooling, the evolution of the density n^{**} of a highly excited Sr** level, following the ~10-ns laser pulse, is described by the following rate equation (which ignores cascade effects—see later):

$$\frac{d}{dt}n^{**}=-\Gamma^{**}n^{**}+\tfrac{1}{2}k_{PP}n_P^2 \ . \tag{1}$$

Here Γ^{**} is the radiative decay rate of n^{**}, n_p is the density of the $5\,^1P$ state, and the factor of $\frac{1}{2}$ corrects for double counting of identical particles. Assuming that the decay of the $5\,^1P$ state is dominated by radiative decay rather than collisional (EP) losses (as can be justified *a posteriori),* it is easy to show that

$$n^{**}(t)=\tfrac{1}{2}k_{PP}n_P^2(0)\frac{1}{\Gamma^{**}-2\Gamma^P_{\rm eff}}(e^{-2\Gamma^P_{\rm eff}t}-e^{-\Gamma^{**}t}) \ , \tag{2}$$

where $\Gamma^P_{\rm eff}$ is the effective decay rate of the $5\,^1P$ level, which due to radiation trapping, is generally much smaller than Γ^{**}. The detected EP signal is given by

$$S^{\rm EP}(t)=\epsilon(\lambda_{\rm det})\Gamma^{**}B_\lambda n^{**}(t) \ , \tag{3}$$

where B_λ is the branching ratio for the detected transition and the sensitivity factor $\epsilon(\lambda)$ is determined by the geometry and the spectral response (per photon) of the detection system. The same sensitivity factor applies to the signal for the $5\,^1P$ state resonance fluorescence,

$$S^{\rm RS}(t)=\epsilon(\lambda_{\rm res})\Gamma^P_{\rm eff}n_P(t) \ , \tag{4}$$

where $S^{\rm RS}$ is the detected signal for the resonance fluorescence at $\lambda_{\rm res}$. From Eqs. (3) and (4), the rate coefficient k_{PP} can be expressed as

$$B_\lambda k_{PP}=2\frac{S^{\rm EP}/\epsilon(\lambda_{\rm det})}{S^{\rm RS}/\epsilon(\lambda_{\rm res})}\frac{\Gamma^P_{\rm eff}}{n_P}\left[1-2\frac{\Gamma^P_{\rm eff}}{\Gamma^{**}}\right]\frac{1}{1-e^{(2\Gamma^P_{\rm eff}-\Gamma^{**})t}} \ . \tag{5}$$

In the present experiment the resonance fluorescence is radiatively trapped, leading to $\Gamma^{**}\gg\Gamma^P_{\rm eff}\sim10^6\ {\rm s}^{-1}$. At times $t\gg1/\Gamma^{**}$, $S^{\rm EP}$ follows a simple exponential behavior (decay rate $2\Gamma^P_{\rm eff}$) and the last factor on the right-hand side of Eq. (5) can be neglected.

In a similar manner we obtain the following expression for the rate coefficient k_{DD} with the EP signal again measured relative to $S^{\rm RS}(t)$:

$$B_\lambda k_{DD}=2\frac{S^{\rm EP}/\epsilon(\lambda_{\rm det})}{S^{\rm RS}/\epsilon(\lambda_{\rm res})}\Gamma^P_{\rm eff}\frac{n_P}{n_D^2} \ . \tag{6}$$

Here n_D is the density of Sr atoms in the $4\,^1D$ state. The factor $1-2\Gamma^D_{\rm eff}/\Gamma^{**}$ is negligible in this case, as a result of the long effective lifetime (determined by wall collisions) of the metastable $4\,^1D$ state.

A. Apparatus

The Sr vapor is contained in a cross-shaped cell, which proved to be a more reliable design from that described in Refs. 9 and 13. As previously, sapphire windows are

sealed to a heated stainless steel block by Ni helicoflex O rings.[15] However, small leaks through these seals can now be tolerated, since a vacuum-tight seal to the outside world is realized by cold windows on conflat flanges. With this double-window setup, we have been able to work under buffer-gas-free conditions at 400–700 °C cell temperatures for extended periods. In the present experiment it is essential to work without buffer gas, since this would cause collisional transfer between the highly excited Sr states before they could decay radiatively. The interaction volume is well defined by inserting sapphire rods (12.5-mm diam) inside the hot sapphire windows to fill all but 6.5-mm gap (see Fig. 3 in Ref. 6). In this way absorption of fluorescence light due to Sr vapor outside the interaction volume is eliminated. The temperature of the cell is typically 770 K in the present experiments, a side arm containing the Sr metal being at ~50 K lower temperature; this yields a Sr density on the order of 10^{13} cm^{-3}.

The $5\,^1P$ level is excited by a ~6-ns, ~0.1-mJ pulse of a Nd:YAG (where YAG denotes yttrium aluminum garnet) pumped dye laser, which is normally spatially expanded to nearly fill (~5 mm wide and ~12 mm high) the interaction volume. The dye laser output has a spectrally broad, low-intensity contribution due to amplified spontaneous emission from the dye cell. Since this light can produce additional population in highly excited states via two-photon excitation, the spectral output of the dye laser was "cleaned up" by passing the beam through two dispersing prisms and a spatial filter.

When the Sr density, laser power, and detuning are adjusted to produce a particular threshold Sr($5\,^1P_1$) density, the metastable $4\,^1D_2$ level becomes strongly populated during the laser pulse by stimulated $5\,^1P \rightarrow 4\,^1D$ emission. The resulting densities of Sr atoms in the $5\,^1P$ and $4\,^1D$ levels are obtained from the absorption of narrow spectral lines from a Sr hollow cathod lamp, connecting those states to higher-lying states (Figs. 1 and 3 and Table I). The lamp light is focused to a 3-mm-diam spot in the center of the interaction volume, and after passage through the cell is refocussed onto the entrance slit of a monochromator. The emission lines of the lamp have a ~300-K Doppler profile,[9] whereas the Sr in the cell has 770-K Doppler-broadened absorption lines. Therefore spectral integration of 770-K Doppler absorption of a 300-K Doppler line is used to transform measured fractional absorption to excited-state density. In the experiment, care is taken to insure that fractional absorption normally does not exceed ~80%, as the exact form of both line-wing shapes and the small fraction of other isotopes is then more critical. The $5\,^1P$ density immediately after the laser pulse is typically $(3-12)\times10^{11}$ cm^{-3}, while the $4\,^1D$ density is $(0-9)\times10^{11}$ cm^{-3}.

A $\frac{3}{4}$-m double monochromator and a photomultiplier are used to detect the lamp light and the fluorescence light emitted by the Sr vapor in the cell. The amplified photomultiplier output is processed by a fast transient digitizer and the time-resolved signals, which are typically averaged over 10^3-10^4 pulses, are stored in a computer for later analysis. Measuring time-resolved signals for all Sr** states with the transient digitizer would have been

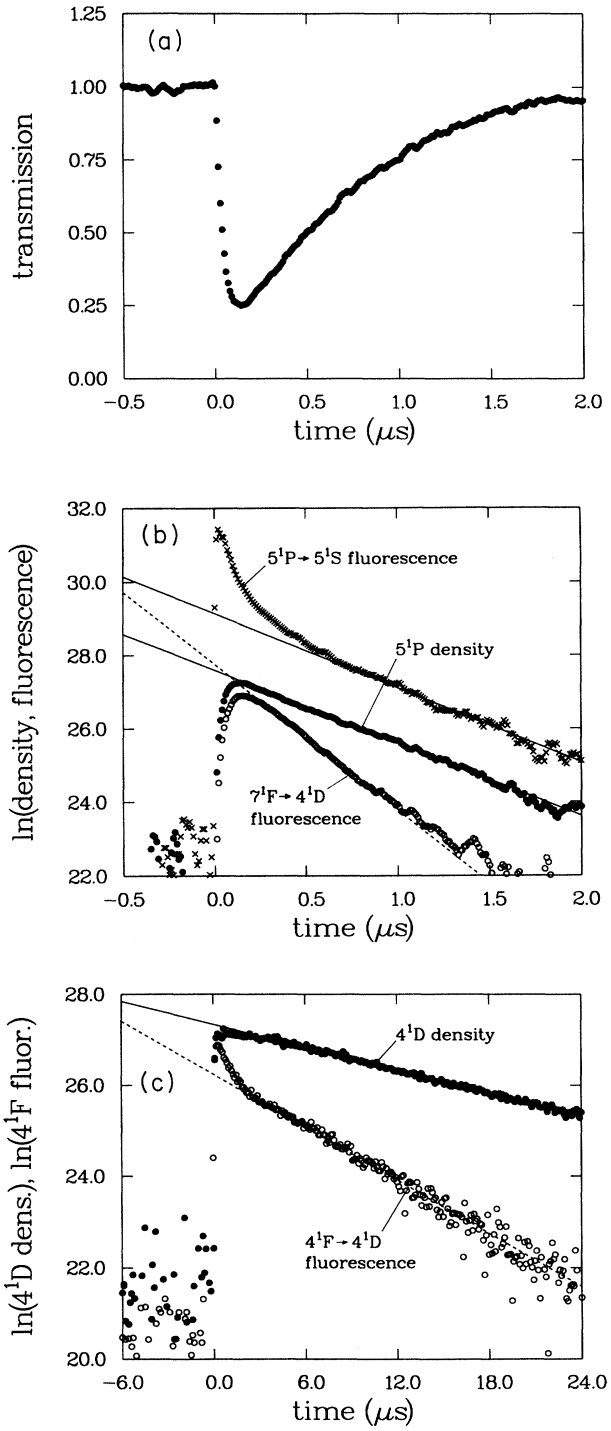

FIG. 3. Example of a time-dependent measurement of densities and fluorescence intensities. (a) Transmission through the cell of the 7673-Å light from a Sr hollow-cathode lamp, connecting the $5\,^1P$ and $5\,^1D$ levels. (b) $5\,^1P$ density [in cm^{-3} units, calculated from (a)] and measured $5\,^1P$ and $7\,^1F$ fluorescence intensities on a semilogarithmic scale. The solid lines correspond to a decay rate of 2.0×10^6 s^{-1} (Γ^P_{eff}) and the dashed line to a decay rate of 4.0×10^6 s^{-1}. (c) $4\,^1D$ density, in cm^{-3} units, and $4\,^1F$ fluorescence on a semilogarithmic scale. The solid and dashed lines correspond to decay rates of 0.86×10^5 and 2.0×10^5 s^{-1}, respectively.

TABLE I. Absorption lines used to measure the $5\,^1P$ and $4\,^1D$ densities.

λ (Å)	Lower state	Upper state	τ (upper state) (ns)	B_λ	A (10^7 s^{-1})
7673	$5\,^1P_1$	$5\,^1D_2$	115±5.8[b]	1.00	0.87
7309	$4\,^1D_2$	$4d5p\,^1D_2$	21.9±1.5[b]	0.85[c]	3.9

[a]Reference 21.
[b]Reference 22.
[c]Reference 16.

very time consuming, so a gated integrator was used to average the photomultiplier signal during either of two time intervals after the laser pulse, as will be discussed below. By scanning the monochromator we obtained a fluorescence spectrum during each time interval (Fig. 4). From these spectra it is determined which Sr** levels are populated by EP collisions.

B. Measurements

Since the lifetimes of the highly excited states are much shorter than the effective lifetimes of the $5\,^1P$ and $4\,^1D$ states, the fluorescence originating from the states produced by EP essentially follows the instantaneous production rate. The effective lifetime of the $5\,^1P$ level is 0.5–1 μs due to strong radiation trapping (the natural lifetime is $\sim$5 ns), whereas the effective lifetime of the $4\,^1D$ level, from wall collisions, is $\sim$10 μs. Therefore, from the temporal behavior of a fluorescence from a certain highly excited state, it can be seen immediately which pair of collision partners, i.e., $5\,^1P+5\,^1P$, $5\,^1P+4\,^1D$, or $4\,^1D+4\,^1D$, is responsible for the population of that state (Fig. 3).

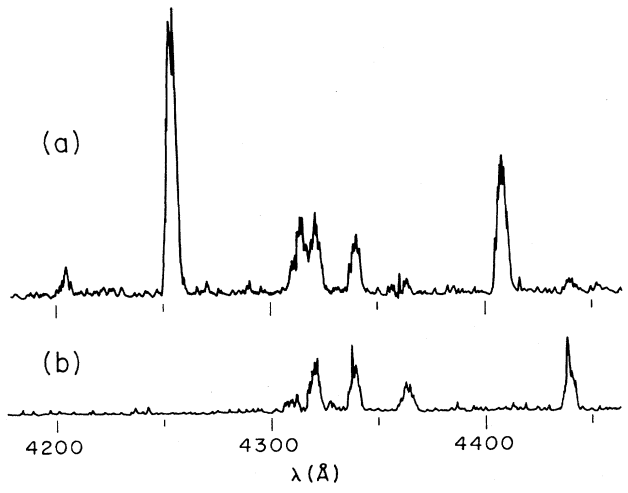

FIG. 4. Partial fluorescence spectra obtained using a gated integrator averaging the photomultiplier signal during a fixed time interval after the laser pulse. (a) For $5\,^1P+5\,^1P$ energy pooling (integrator gate open from 0.16 until 0.60 μs, $4\,^1D$ density $\sim$3% of the $5\,^1P$ density). (b) The same for $4\,^1D+4\,^1D$ energy pooling (integrator gate open from 4.0 until 6.0 μs, $5\,^1P$ density $\sim$1% of the $4\,^1D$ density).

From Eqs. (5) and (6) we see that the rate coefficients can be derived from a ratio of fluorescence intensities, the absolute densities of atoms in the $5\,^1P$ and $4\,^1D$ levels, and the effective decay rate of the $5\,^1P$ state. These densities and decay rate are determined from the absorption measurements using the hollow-cathode lamp. The spectral sensitivity per photon $\epsilon(\lambda)$ in Eqs. (3)–(6) is obtained from a calibration using a calibrated tungsten iodide lamp. Since the lamp has a continuous spectrum and atomic lines are monochromatic, this includes dividing the lamp intensity per wavelength interval $I^w(\lambda)$ (in W/cm^2 Å) by the monochromator dispersion $D(\lambda)$. Using the same geometrical arrangement as during the energy pooling measurements, we determine $\epsilon(\lambda)$ from

$$\epsilon(\lambda)=[CS^w(\lambda)D(\lambda)]/[I^w(\lambda)\lambda]\ . \tag{7}$$

Here $S^w(\lambda)$ is the observed photomultiplier signal and C is a wavelength-independent factor, which is arbitrary, since only a ratio of spectral sensitives is used in our analysis [Eqs. (5) and (6)].

For the case of $5\,^1P+5\,^1P$ energy pooling we have determined the absolute rate coefficient for the $7\,^1F$ level, while the $4\,^1F$ level was chosen as the reference level for $4\,^1D+4\,^1D$ energy pooling. In each case the full time-dependent signals were studied and analyzed. From Fig. 3(b) we see that the $7\,^1F\rightarrow 4\,^1D$ fluorescence decays twice as fast as the $5\,^1P$ density and the $5\,^1P\rightarrow 5\,^1S$ resonance fluorescence, indicating that the $7\,^1F$ level is primarily populated by $5\,^1P+5\,^1P$ energy pooling. (From the data we find that the contribution of $5\,^1P+4\,^1D$ EP is less than 5%.) The resonance fluorescence has a nonexponential behavior until $\sim$1 μs after the laser pulse, corresponding to decay of the fundamental spatial mode (see later) and consistent with the optical depth that accompanies the significant fraction of excited Sr atoms. From Fig. 3(c) we see that the decay of the $4\,^1F\rightarrow 4\,^1D$ fluorescence has a fast feature until $\sim$2 μs after the laser pulse, probably due to cascade from higher levels which were populated through $5\,^1P+5\,^1P$ and $5\,^1P+4\,^1D$ energy pooling. After the initial $\sim$2 μs the fluorescence decays slightly more than two times faster than the measured $4\,^1D$ density. This might be due to the fact that the $4\,^1F$ production rate is dependent on the relative velocity of the colliding $4\,^1D$ atom pairs. The $4\,^1D$ population dominantly decays through wall collisions, and since fast atoms on the average reach the wall sooner than slow atoms, the velocity distribution of the $4\,^1D$ atoms narrows in time. (This effect has not been taken into account when determining

the $4\,^1D$ density using the two Doppler absorption formulas, but is estimated to be an insignificant correction.) Furthermore, the spatial distribution of the $4\,^1D$ atoms changes as well, which will also affect the $4\,^1F$ production rate (see Sec. III). Since we determined the absolute rate coefficient for the $4\,^1F$ level from signals ~ 2 μs after the laser pulse, these effects play a negligible role ($\sim 5\%$ correction).

All other rate coefficients were determined relative to these reference values using the gated integrator, as mentioned above. By varying the detuning and the intensity of the laser we could produce conditions where the initial $4\,^1D$ density was negligible compared to the $5\,^1P$ density. Under these conditions we opened the integrator gate from 0.16 μs until 0.60 μs after the laser pulse, collecting most of the Sr**signals resulting from $5\,^1P+5\,^1P$ energy pooling. Under excitation conditions (varying laser detuning and intensity) such that immediately after the laser pulse the $4\,^1D$ and $5\,^1P$ densities are of the same magnitude (the ground-state density being unchanged), we used an integrator gate which is open from 4.0 μs until 6.0 μs after the laser pulse to detect only $4\,^1D+4\,^1D$ EP signals. During this time interval the $5\,^1P$ density is negligible compared to the $4\,^1D$ density, due to the effective decay rates which differ by a order of magnitude. (Under these conditions strong fluorescence at 4962 Å proportional to the $4\,^1$D density was observed and attributed to the $4\ ^1D \rightarrow 5\,'S$ electric quadrupole transition. This yields a radiative decay rate for this transition, which will be given in Ref. 16.)

In the case of $5\,^1P+5\,^1P$ energy pooling the unknown rate coefficients are related to the reference-state rate coefficient by

$$B_\lambda k_{PP} = B_\lambda^{\rm ref} \frac{S^{\rm EP}/\epsilon(\lambda)}{S_{\rm ref}^{\rm EP}/\epsilon(\lambda_{\rm ref})} f(\Gamma^{**}, \Gamma^{\rm ref}, \Gamma_{\rm eff}^{P}) \ , \tag{8}$$

where $\Gamma^{\rm ref}$ is the radiative decay rate of the reference level, i.e., $7\,^1F$ or $4\,^1F$. The decay-rate correction factor $f(\Gamma^{**}, \Gamma^{\rm ref}, \Gamma_{\rm eff}^{P})$ varies from ~ 1.0 to 1.6 for the final states studied and can easily be derived by integrating Eq. (5) from 0.16 until 0.6 μs. In the case of $4\,^1D+4\,^1D$ energy pooling a similar expression is obtained, with $f(\Gamma^{**}, \Gamma^{\rm ref}, \Gamma_{\rm eff}^{D}) \approx 1$.

III. ANALYSIS

From the present experiment we obtain products $B_\lambda k(n^{2S+1}L)$, where B_λ is the radiative branching, since for each highly excited state only fluorescence from one decay channel is normally detected. This is due to the fact that other transitions from the given highly excited state radiate outside the measured wavelength region of 330–800 nm. Furthermore, decay of more-highly-excited states may feed the state of interest, and the resulting additional fluorescence due to cascade will add to that due to direct energy pooling into this state. To obtain the direct rate coefficients $k(n^{2S+1}L)$ and to estimate the contribution of cascading population to the observed fluorescence intensities, knowledge of the radiative branching ratios is required. Previous work on Sr lifetimes and oscillator strengths was highly incomplete for the transitions of interest. Therefore, we have calculated most of the missing oscillator strengths using the Coulomb approximation.[17] The Coulomb approximation cannot be used for transitions connecting to the $4\,^1D$ and $4\,^3D$ levels, so these were obtained from a multichannel quantum defect theory calculation, the results of which will be published separately.[16]

When analyzing the data, attention should be paid to a few complications which have not been mentioned so far.

(i) In deriving Eqs. (5) and (6) we have assumed that the densities of the $5\,^1P$ and $4\,^1D$ atoms are spatially uniform, which is certainly not the case. The vapor-filled gap between the sapphire rods is half of the rod diameter, approximating a one-dimensional "slab" geometry. The laser beam fills the full height of the rod diameter, so that it initially excites a nearly uniform distribution in the plane parallel to the sapphire-rod faces. Thus, we approximate the density distributions as one dimensional. As far as the $5\,^1P$ state is concerned, Holstein's theory of radiation trapping[18,19] indicates that in the early time after excitation many (one-dimensional) spatial modes with different time dependencies can be excited. The higher-order modes decay faster than the fundamental mode, which eventually will dominate the decay. In order to minimize the time required for the $5\,^1P$ density to reach this fundamental-mode decay rate, a laser beam is used which fills $\sim 80\%$ of the gap between the windows, thereby maximizing the overlap of the beam with the fundamental-mode distribution.[4,20] As we can see from Fig. 3(b) nearly single-exponential decay for the $5\,^1P$ density is indeed observed in our experiments. The initial spatial distribution of $4\,^1D$ atoms, which are produced by a stimulated process during the laser pulse, is more sharply peaked at the center, since it depends on the geometry of the column of excited $5\,^1P$ atoms in the cell.

From the absorption of the hollow-cathode-lamp lines we obtain average $5\,^1P$ and $4\,^1D$ densities along the path of the lamp light across the gap between the sapphire rods. The Sr** fluorescence, however, is proportional to the average of these densities squared along this path. When inserting these average density values into Eqs. (5) and (6), we should correct for the difference between the average of the density squared and the square of the average density. For this correction for the $5\,^1P$ density, we assume a fundamental-mode spatial distribution, calculated by van Trigt[20] for an infinite-slab geometry. This yields a correction factor of ~ 0.85 that multiplies the right-hand side of Eq. (5). This correction for the $4\,^1D+4\,^1D$ EP data has been estimated from a measurement of the $4\,^1D$ density versus vertical position, under conditions where the vertical dimension of the laser beam was the same (~ 5 mm) as the horizontal dimension. This $4\,^1D$ distribution had a $\sim$4-mm halfwidth, producing a correction factor for Eq. (6) of ~ 0.8.

(ii) Due to the initial density of the $5\,^1P$ and $4\,^1D$ states, radiation trapping of Sr** fluorescence light connecting

TABLE II. $5\,^1P+5\,^1P$ energy pooling [$2\times E(5\,^1P)=43\,397$ cm^{-1}]. Dashes denote highly uncertain values.

Upper level	E (cm^{-1})	Lower level	λ_{det} (Å)	$\frac{S_{ep}/\epsilon(\lambda)}{S_{ref}/\epsilon(\lambda_{ref})}$	$B_\lambda k_{pp}^{(0)}$ [a] (10^{-11} cm^3/s)	B_λ [b]	$k_{pp}^{(0)}$ [a] (10^{-11} cm^3/s)	Cascade[c]	$f(\Gamma^{**})$	k_{pp} (10^{-11} cm^3/s)
$11\,^1P$	44 366	$4\,^1D$	4128	0.01±0.01	0.04±0.04	0.37	0.10	0.00	1.00	0.1±0.1
$11\,^3P$	44 267	$4\,^3D$	3830	<0.01	<0.04	–		0.00		
	(avg.)		3838							
$8\,^1F$	44 190	$4\,^1D$	4159	0.11±0.03	0.39±0.15	0.91	0.43	0.00	1.06	0.46±0.18
$8\,^3F$	44 172	$4\,^3D$	3843	0.09±0.04	0.32±0.16	0.97	0.33	0.00	1.04	0.34±0.17
	(avg.)		3852							
			3867							
$11\,^1S$	44 097	$5\,^1P$	4463	0.02±0.01	0.07±0.04	0.46	0.15	0.00	1.31	0.20±0.12
$11\,^3S$	44 043	$5\,^3P$	3357	<0.01	<0.04	–				
			3378							
			3424							
$10\,^1P$	43 936	$4\,^1D$	4203	0.08±0.03	0.28±0.13	0.38	0.75	0.00	1.00	0.8±0.4
$9\,^3D$	43 810	$5\,^3P$	3412	0.06±0.04	0.22±0.16	0.74	0.30	<0.1	1.09	0.3±0.2
	(avg.)		3458							
$10\,^3P$	43 765	$4\,^3D$	3905	<0.01	<0.04	–				
	(avg.)		3914							
$9\,^1D$	43 756	$5\,^1P$	4532	0.07±0.02	0.24±0.11	0.57	0.42	0.01	1.37	0.6±0.3
$7\,^1F$	43 656	$4\,^1D$	4253	1.00	3.5±1.1	0.89	3.9	0.00	1.00	3.9±1.3
$7\,^3F$	43 624	$4\,^3D$	3926	0.43±0.12	1.5±0.6	0.93	1.6	0.00	1.00	1.6±0.7
	(avg.)		3935							
			3951							
$10\,^1S$	43 512	$5\,^1P$	4583	0.11±0.06	0.39±0.25	0.48	0.81	0.00	1.19	1.0±0.7
$10\,^3S$	43 428	$5\,^3P$	3434	0.12±0.09	0.4±0.03	0.63	0.7	<0.2	1.09	0.7±0.6
			3456							
			3504							
$9\,^1P$	43 328	$4\,^1D$	4313	0.24±0.12	0.8±0.5	0.41	2.1	0.02	1.06	2.2±1.3
$8\,^3D$	43 072	$5\,^3P$	3477	0.20±0.06	0.71±0.30	0.76	0.93	<0.2	1.00	0.8±0.5
	(avg.)		3500							
			3548							
$8\,^1D$	43 021	$5\,^1P$	4689	0.16±0.06	0.57±0.27	0.64	0.89	0.15	1.05	0.8±0.4
$9\,^3P$	42 990	$6\,^3S$	7166	? overlap		0.04				
$6\,^1F$	42 840	$4\,^1D$	4406	0.57±0.10	2.0±00.7	0.86	2.3	e	1.01	
$6\,^3F$	42 777	$4\,^3D$	4061	0.40±0.10	1.4±0.6	0.92	1.5	e	1.01	
	(avg.)		4071							
			4087							
$9\,^1S$	42 597	$5\,^1P$	4784	0.08±0.02	0.30±0.12	0.50	0.60	0.00	1.00	0.6±0.3
$8\,^1P$	42 462	$4\,^1D$	4481	0.12±0.03	0.44±0.17	0.46	0.96	0.06	1.09	1.0±0.4
$9\,^3S$	42 451	$5\,^3P_1$	3577	0.03±0.03	0.11±0.11	0.64	0.17	–	1.01	<0.2
$7\,^3D$	41 870	$5\,^3P$	3629	0.37±0.09	1.3±0.5	0.80	1.6	<0.5	1.01	1.3±0.6
	(avg.)		3653							
			3706							

TABLE II. (*Continued*).

Upper level	E (cm^{-1})	Lower level	λ_{det} (Å)	$\frac{S_{ep}/\epsilon(\lambda)}{S_{ref}/\epsilon(\lambda_{ref})}$	$B_\lambda k_{pp}^{(0)}$ [a] (10^{-11} cm^3/s)	B_λ [b]	$k_{pp}^{(0)}$ [a] (10^{-11} cm^3/s)	Cascade	$f(\Gamma^{**})$	k_{pp} (10^{-11} cm^3/s)
$7\,^1D$	41 831	$5\,^1P$	4966	? overlap		0.73		0.26	1.00	
$8\,^3P$	41 720	$4\,^3D$	4243	<0.01	<0.04	0.13	<0.3	0.08	1.64	<0.3
	(avg.)		4269							
$5\,^1F$	41 519	$4\,^1D$	4678	0.62±0.11	2.2±0.8	0.80	2.7	e	1.06	
$5\,^3F$	41 366	$4\,^3D$	4308	0.59±0.15	2.1±0.8	0.88	2.4	e	1.05	
	(avg.)		4319							
			4338							
$4d5p\,^1P$	41 172	$4\,^1D$	4755	0.10±0.03	0.37±0.15	0.59	0.63	—	1.10	
$8\,^1S$	41 052	$5\,^1P$	5166	0.05±0.03	0.18±0.12	0.48	0.38	0.00	1.01	0.4±0.3
$8\,^3S$	40 763	$5\,^3P_1$	3807	0.02±0.01	0.06±0.04	0.66	0.09	—	1.01	<0.1
$6\,^1D$	39 733	$5\,^1P$	5543	0.38±0.07	1.3±0.5	0.76[d]	1.8	0.44	1.06	1.4±0.8
$6\,^3D$	39 696	$5\,^3P$	3969	0.25±0.08	0.89±0.40	0.87	1.0	—	1.05	
	(avg.)		4030							
$4\,^1F$	39 539	$4\,^1D$	5156	0.40±00.07	1.4±0.5	0.58	2.4	e	1.08	
$7\,^3P$	39 442	$4\,^3D$	4714	0.14±0.07	0.50±0.28	0.52	0.96	0.27	1.12	0.8±0.6
	(avg.)		4729							
$7\,^1P$	38 907	$4\,^1D$	5329	0.20±0.04	0.70±0.25	0.80	0.88	0.41	1.07	0.5±0.4
$4\,^3F$	38 753	$4\,^3D$	4855	0.8±0.3	2.8±1.4	0.79	3.6	e	1.09	
	(avg.)		4869							
			4893							
$7\,^1S$	38 444	$5\,^1P$	5970	0.04±0.03	0.15±0.12	0.62	0.24	0.02	1.11	0.25±0.20
$4d5p\,^1F$	38 008	$4\,^1D$	5598	0.07±0.03	0.24±0.12	1.00	0.24	e	1.18	
$7\,^3S$	37 425	$5\,^3P_2$	4438	0.03±0.01	0.11±0.05	0.72	0.15	>0.2	1.06	
$4d5p\,^3P$	37 320	$4\,^3D$	5225	0.11±0.06	0.4±0.3	1.00	0.4	—	—	
	(avg.)		5239							
			5257							
								total rate coefficient:		36±13

[a]Uncorrected for cascade contribution and effect of Sr^{**} decay rate.

[b]MODT calculation for $n\,^1P \rightarrow 5\,^1S$, $6\,^1S$, $5p^2\,^1S$, $4\,^1D$, $5\,^1D$; $n\,^1F \rightarrow 4\,^1D$; $n\,^3P \rightarrow 6\,^3S$, $4\,^3D$; $n\,^3F \rightarrow 4\,^3D$. Coulomb approximation (Ref. 15) for all other transitions (Ref. 16).

[c]Calculated from observed lines only.

[d]Corrected for radiation trapping.

[e]Possibly large cascade contribution from $1,3G$ and $^{1,3}H$ states.

TABLE III. $4\,^1D+4\,^1D$ energy pooling [$2\times E(4\,^1D)=40\,299\ \mathrm{cm}^{-1}$]. Dashes denote highly uncertain values..

Upper level	E (cm^{-1})	Lower level	λ_{det} (Å)	$\frac{S_{ep}/\epsilon(\lambda)}{S_{ref}/\epsilon(\lambda_{ref})}$	$B_\lambda k_{DD}^{(0)}$ [a] (10^{-11} cm^3/s)	B_λ [b]	$k_{DD}^{(0)}$ [a] (10^{-11} cm^3/s)	Cascade[c]	k_{pp} (10^{-11} cm^3/s)
$7\,^3D$	41 870	$5\,^3P$	3629	0.03±0.02	0.13±0.10	0.80	0.16	0.00	0.16±0.13
	(avg.)		3653						
			3706						
$7\,^1D$	41 831	$5\,^1P$	4966	? overlap		0.73		0.00	
$8\,^3P$	41 720	$4\,^3D$	4243	<0.003	<0.01	0.13	<0.1	0.00	<0.1
	(avg.)		4254						
			4272						
$5\,^1F$	41 519	$4\,^1D$	4678	0.10±0.03	0.43±0.21	0.74[d]	0.58	0.00	0.6±0.3
$5\,^3F$	41 366	$4\,^3D$	4308	0.26±0.05	1.1±0.5	0.88	1.3	0.00	1.3±0.6
	(avg.)		4319						
			4338						
$4d5p\,^1P$	41 172	$4\,^1D$	4755	0.11±0.02	0.47±0.23	0.59	0.80	0.00	0.8±0.4
$8\,^1S$	41 052	$5\,^1P$	5166	0.02±0.01	0.09±0.06	0.48	0.18	0.00	0.18±0.13
$8\,^3S$	40 763	$5\,^3P$	3780	0.07±0.03	0.30±0.17	0.66	0.45	0.00	0.5±0.3
			3807						
			3865						
$6\,^1D$	39 733	$5\,^1P$	5543	0.63±0.14	2.7±1.2	0.81	3.4	0.08	3.3±1.6
$6\,^3D$	39 696	$5\,^3P$	3941	0.61±0.12	2.6±1.2	0.87	3.0	0.12	2.9±1.5
	(avg.)		3969						
			4030						
$4\,^1F$	39 539	$4\,^1D$	5156	1.00	4.3±1.7	0.48[d]	9.1	0.00	9.1±3.6
$7\,^3P$	39 442	$4\,^3D$	4704	0.23±0.05	0.99±0.46	0.52	1.9	0.06	1.8±1.0
	(avg.)		4714						
			4729						
$7\,^1P$	38 907	$4\,^1D$	5329	0.26±0.03	1.12±0.47	0.76[d]	1.5	0.07	1.4±0.6
$4\,^3F$	38 753	$4\,^3D$	4855	0.8±0.2	3.4±1.7	0.79	4.4	0.02	4.4±2.2
	(avg.)		4869						
			4892						
$7\,^1S$	38 444	$5\,^1P$	5970	0.06±0.02	0.26±0.16	0.62	0.42	0.00	0.4±0.3
$4d5p\,^1F$	38 008	$4\,^1D$	5598	0.14±0.03	0.60±0.27	1.00	0.60	—	
$7\,^3S$	37 425	$5\,^3P$	4325	0.22±0.07	0.95±0.47	0.72	1.3	0.5	0.8±0.6
			4362						
			4438						
$4d5p\,^3P$	37 320	$4\,^3D$	5225	0.24±0.05	1.03±0.46	1.00	1.0	—	
	(avg.)		5239						
			5257						
$5p^2\,^1S$	37 160	$5\,^1P$	6466	0.07±0.04	0.30±0.22	1.00	0.30	—	
$5p^2\,^1D$	36 961	$5\,^1P$	6550	0.21±0.09	0.9±0.5	1.00	0.9	—	
$4d5p\,^3D_3$	36 560	$4\,^3D$	5451	0.22±0.05	0.70±0.33	—			
			5481						

TABLE III. (*Continued*).

Upper level	E (cm^{-1})	Lower level	λ_{det} (Å)	$\frac{S_{ep}/\epsilon(\lambda)}{S_{ref}/\epsilon(\lambda_{ref})}$	$B_\lambda k_{DD}^{(0)}$ [a] (10^{-11} cm^3/s)	$\frac{k_{pp}^{(0)}}{B_\lambda}$ [a] [b]	(10^{-11} cm^3/s)	Cascade[c]	k_{pp} (10^{-11} cm^3/s)
$4d5p\,^3D_2$	36 382	$4\,^3D$	5486	0.19±0.06	0.62±0.32	–			
			5504						
			5535						
$4d5p\,^3D_1$	36 264	$4\,^3D$	5522	0.14±0.08	0.5±0.3	–			
			5540						
$5p^2\,^3P_2$	35 675	$5\,^3P$	4722	0.19±0.04	0.82±0.37	1.00	0.82	–	
			4812						
$5p^2\,^3P_1$	35 400	$5\,^3P_0$	4742	0.04±0.02	0.17±0.09	1.00	0.17	–	
$5p^2\,^3P_0$	35 193	$5\,^3P_1$	4832	? overlap		1.00		–	
$5\,^3D$	35 030	$5\,^3P$	4832	? overlap		1.00		1.1	
	(avg.)		4873						
			4876						
			4963						
			4968						
			4972						
$5\,^1D$	34 727	$5\,^1P$	7673	2.1±0.3	9.0±3.9	0.99	9.1	4.9	
$6\,^1P$	34 098	$4\,^1D$	7167	0.10±0.05	0.43±0.27	0.60[d]	0.72	0.66	0.1±0.4
							total rate coefficient:		28±13

[a] Uncorrected for cascade contribution.

[b] MODT calculation for $n\,^1P \rightarrow 5\,^1S$, $6\,^1S$, $5p^2\,^1S$, $4\,^1D$, $5\,^1D$; $n\,^1F \rightarrow 4\,^1D$; $n\,^3P \rightarrow 6\,^3S$, $4\,^3D$; $n\,^3F \rightarrow 4\,^3D$. Coulomb approximation (Ref. 15) for all other transitions (Ref. 16).

[c] Calculated from observed lines only.

[d] Corrected for radiation trapping.

to these levels might occur. If the fluorescence also branches to other states (e.g., $4\,^1F$ radiates to $4\,^1D$ and $5\,^1D$), this radiation trapping will alter the branching ratios and thus change the observed fluorescent intensity. As an example, when determining the absolute $4\,^1D+4\,^1D\rightarrow 4\,^1F+5\,^1S$ rate coefficient, the detected $4\,^1F\rightarrow 4\,^1D$ fluorescence (515 Å, see Table III) typically had a measured (on resonance) optical depth across the cell of ~ 0.5 (corresponding to an average $4\,^1D$ density of $\sim 5.6\times 10^{11}$ cm^{-3}). By assuming Gaussian emission and absorption profiles we estimate the average probability that a fluorescent photon is absorbed by the $4\,^1D$ atoms before it escapes out of the cell. Using this and the fact that every time the fluorescent light is reabsorbed it is again emitted as $4\,^1F\rightarrow 4\,^1D$ fluorescence with the natural (unperturbed) branching ratio, $B_\lambda \approx 0.58$,[16] we estimate that in this case the effective branching ratio is $\sim 7\%$ smaller than the unperturbed value. Corrections due to radiation trapping have also been applied to the branching ratios shown in column 7 of Tables II and III. These corrections are smaller than 20% in all cases and negligible for most of them.

(iii) We have attempted to correct for cascade effects by taking into account the observed population of all higher-lying states and by using our estimate[16] of the radiative branching ratios of those states. However, fluorescence from high angular momentum ($L=4$, 5, etc.) states cannot be detected in our experiment, so that most cascade from such states into the $^{1,3}F$ states in included in the apparent F-state rate coefficients. Since the $5G$ states lie ~ 1200 cm^{-1} (2.2 kT) above $2\times E(4\,^1D)$, whereas the $6G$ states lie even higher (~ 1400 cm^{-1}), we assume that $G\rightarrow F$ cascade only plays a minor role in the case of $4\,^1D+4\,^1D$ energy pooling. In the case of $5\,^1P+5\,^1P$ energy pooling, however, large effects are likely to occur. Using Coulomb approximation oscillator strengths for the F-G transitions and assuming that the EP population of the G states is comparable to that of the near-lying F states, we estimate that in this case on the order of 20% of the population of the $6\,^{1,3}F$ states is the result of cascade, whereas the $5\,^{1,3}F$ and $4\,^{1,3}F$ states might be dominantly filled by cascade rather than direct energy pooling from the $5\,^1P$ state. Due to the long lifetime of the high-angular-momentum states (>0.3 μs), cascading into lower F states will also take place at relatively late times. As a result, the F-state fluorescence shows a decay slower than what would be the case if the F state were populated by direct energy pooling only. A measurement of the time dependence of the $4\,^1F$ decay fluorescence in the case of $5\,^1P+5\,^1P$ energy pooling (with $4\,^1D$ density negligible) indeed shows clear evidence of cascade feeding. The observed fluorescence had a decay rate three times smaller than would be expected if the $4\,^1F$ state were populated only by direct energy pooling. Due to the ~ 0.5-μs effective limit to the $5\,^1P+5\,^1P$ data collection, only thermal-radiation-induced Sr** transfer within that time is relevant; estimates show this to be negligible.

IV. RESULTS

Measurements of the absolute rate coefficients for the $7\,^1F$ and $4\,^1F$ reference levels were repeated 15 and eight times, respectively. By varying laser intensity (within a factor of 8 in the case $4\,^1D+4\,^1D\rightarrow 4\,^1F+5\,^1S$) and detuning, Sr density and the shape of the laser beam in the cell, the initial $5\,^1P$ and $4\,^1D$ densities were both varied within a factor of 3. The following rate coefficient for $5\,^1P+5\,^1P$ collisions producing Sr in the $7\,^1F$ state was found:

$$B_\lambda k_{PP}=(3.5\pm 1.1)\times 10^{-11}\ \text{cm}^3/\text{s}\ .$$

Similarly for $4\,^1D+4\,^1D$ collisions producing $4\,^1F$ atoms:

$$B_\lambda k_{DD}=(3.9\pm 1.6)\times 10^{-11}\ \text{cm}^3/\text{s}\ .$$

Here B_λ is the radiative branching ratio in the absence of radiation trapping.[16] The measured rate coefficients typically fluctuated by $\pm 20\%$ but did not show any systematic behavior as a function of the varied parameters. The 30% and 40% uncertainties in the values given above are a combination of these fluctuations plus uncertainty in the correction factor due to the nonuniform density distributions ($\sim 10\%$) and uncertainties in the $5\,^1P$ and $4\,^1D$ densities. The latter errors are primarily caused by an uncertainty of $\sim 10\%$ in the oscillator strengths used and an uncertainty in the width of the emission lines of the hollow-cathode lamp, also contributing $\sim 10\%$.

The two reference values given above were used to calculate the rate coefficients for other levels from the observed fluorescence intensity ratios. The results are tabulated in Tables II and III, where columns 1 and 3 give the upper and lower levels of the detected fluorescence, respectively. Column 2 contains the energy of the upper level, column 4 the wavelength, column 5 the fluorescence intensity as a ratio of that of the reference line (corrected for the spectral sensitivity of the apparatus), and column 6 the resultant product of branching ratio B_λ and rate coefficient, without taking into account cascading and the factor $f(\Gamma^{**},\Gamma^{\text{ref}},\Gamma^P_{\text{eff}})$ of Eq. (8). Dividing the data of column 6 by our best estimate of the branching ratio, given in column 7 (estimated uncertainty $\sim 20\%$), yields the uncorrected rate coefficient of column 8. An estimate of the cascade contribution is given in column 9. Generally this estimate is based upon the uncorrected results of column 8 for all higher-lying states (if available) and the branching ratios of those states.[16] In the case of $5\,^1P+5\,^1P$ energy pooling (see Table II) rate coefficients for the $11\,^3P$ and $10\,^3P$ states could not be determined due to small branching ratios into the observable fluorescence. For the $9\,^3P$ level the rate coefficient could not be determined due to spectral overlap with another transition. Therefore, cascade contributions to the signals observed from ^3S and ^3D states could not be assessed. However, even the uncorrected rate coefficients $k_{PP}^{(0)}$ (direct energy pooling plus cascade) for the ^3S states are found to be quite small. Based upon these values and the $^3P\rightarrow{}^3S$ and $^3P\rightarrow{}^3D$ branching ratios,[16] we can give upper limits for the cascade contribution to $k_{PP}^{(0)}$ for the $7,8,9\,^3D$ states, which turn out to be relatively small as well. Column 10 in Table II contains the factor $f(\Gamma^{**},\Gamma^{\text{ref}},\Gamma^P_{\text{eff}})$, taking into account the influence of the lifetime of the upper level on the observed signal. Experimental lifetimes were taken from Refs. 21–27. For those levels for which no experimental values were available,

the lifetime was based upon theoretical oscillator strengths,[16] as outlined in Sec. III. The final column of Tables II and III contains the (corrected) direct energy pooling rate coefficients. For some states the absolute uncertainty given here is dominated by the uncertainty in the reference rate coefficient; the uncertainty in the relative rate coefficient is then much smaller. Energy levels above 42 000 cm^{-1} are not shown in Table III, since the $4\,^1D+4\,^1D$ energy pooling rates for these levels have been measured to be smaller than 5×10^{-13} cm^3/s.

V. DISCUSSION

From the data, shown diagrammatically in Fig. 5, it can be seen that there is not a very strong dependence on the exothermic energy defect ΔE. Energy pooling occurs to many states spanning an energy range of several thousand wave numbers. For positive ΔE (endothermic) the rate coefficient decreases more rapidly with increasing $|\Delta E|$ than for negative ΔE (Fig. 5). This, of course, is due to the fact that for positive ΔE only a fraction of the collisions have sufficient kinetic energy to exit as products with a higher electronic energy. The fraction of collision pairs with a relative kinetic energy higher than ΔE is indicated by the dashed line in Fig. 5.

Since the atomic collision partners are initially both singlets, the incident $(Sr^*)_2$ molecule is a singlet as well. However, the separating Sr+Sr* molecule is a singlet or triplet, depending on whether Sr** is a singlet or triplet. Thus, if total spin were conserved, one would not expect triplet Sr** states to be produced. However, there is no indication that the total spin is conserved in the energy transfer; both singlet and triplet states are observed in comparable amounts. For alkaline-earth–noble-gas systems it has already been shown that spin-changing collisions can have large rate coefficients.[28–30] In some cases these rate coefficients are much larger than those for a spin-conserving collision, even when the final singlet state resulting from the latter collision is closer to the initial state.[31,32] Spin-changing collisions are the result of the breakdown of LS coupling, which allows spin-orbit mixing between singlet and triplet states of an isolated atom. The rate coefficients for spin-changing collisions are then mainly determined by the coupling matrix elements at avoided crossings between the molecular potentials connecting to the asymptotic atomic states. The relation between rate coefficient and interaction strength does not display a monotonic behavior, and without accurate knowledge of the numerous potentials involved a prediction of the individual rate coefficients is impossible.

In Figs. 6 and 7, relative EP rate coefficients are indicated by bars for all levels from which fluorescence was observed. The filled portion of a bar corresponds to the direct EP rate coefficient, i.e., after subtraction of the cascade contribution based upon observed population of higher-lying states. The shaded portion indicates the remaining possible estimated contribution to the measured rate from cascade from higher levels for which no fluorescence could be observed. In order to take into account the fact that for positive ΔE only a fraction of the collisions has sufficient relative kinetic energy, the measured rate coefficient has been divided by this fraction. The resulting increase of the endothermic rate coefficient is indicated by the open portion of a bar. A question mark denotes that the rate coefficient could not be determined due to small branching into the observable transition, unknown branching or spectral overlap, or that the population of the level involved was most likely dominated by cascade from higher levels. For uncertainties one should check Tables II and III. From the results for $4\,^1D+4\,^1D$ energy pooling (Fig. 7) we see a clear tendency for the final states to be populated more strongly as their angular momentum increases. This is most likely due to their increasing statistical weight. Such a tenden-

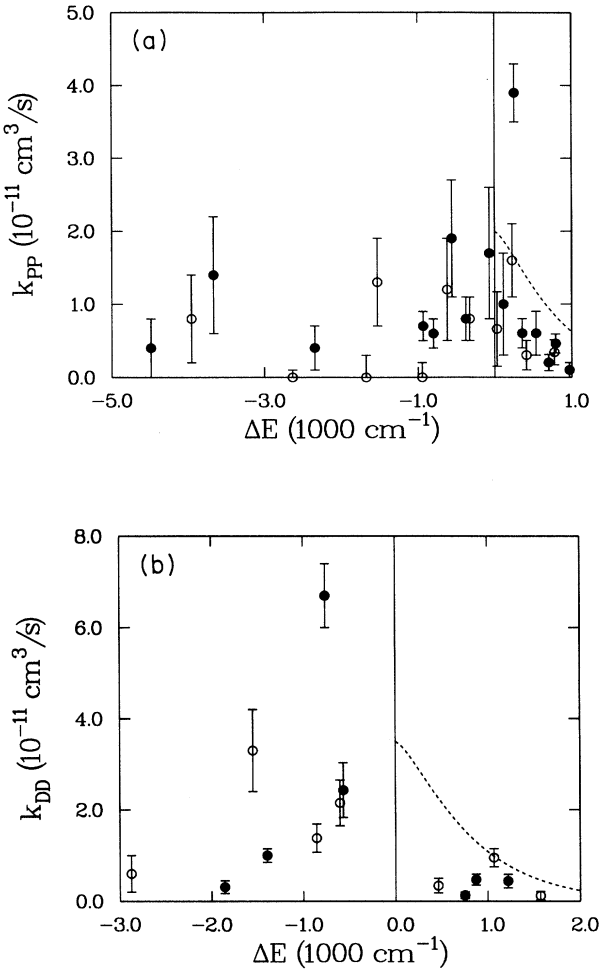

FIG. 5. Relative rate coefficients as a function of the energy defect. Error bars correspond to relative values of the rate coefficients only, absolute errors are significantly larger in some cases. (a) For $5\,^1P+5\,^1P$ energy pooling. (b) For $4\,^1D+4\,^1D$ energy pooling. Solid circles indicate singlet states, open circles triplet states. The dashed curves indicate the fraction of collisions with relative kinetic energy larger than ΔE.

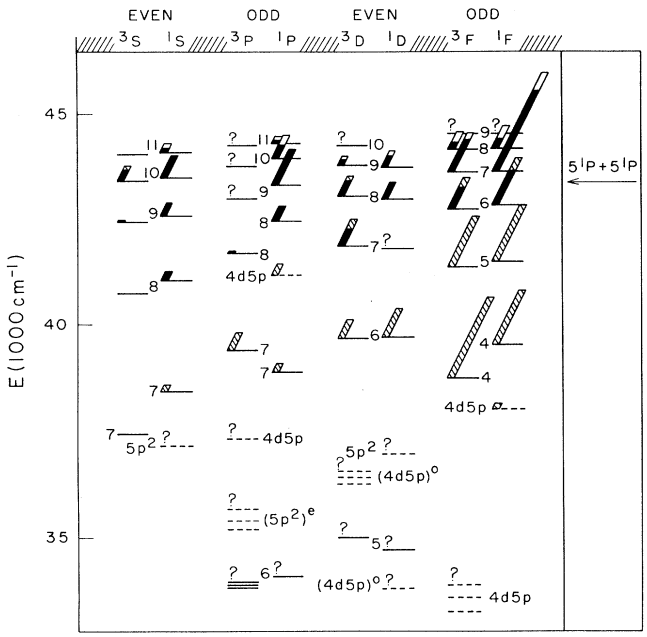

FIG. 6. Relative EP rate coefficients for $5\,^1P+5\,^1P$ energy pooling. The filled portion of a bar corresponds to the direct EP rate coefficient. The shaded portion indicates the possible contribution from cascade. The increase of the rate coefficient above the $5\,^1P+5\,^1P$ threshold, which results from dividing the rate coefficient by the fraction of collisions with sufficient relative kinetic energy, is indicated by the open portion of a bar. A question mark denotes that the rate coefficient could not be determined. Uncertainties are given in Tables II and III.

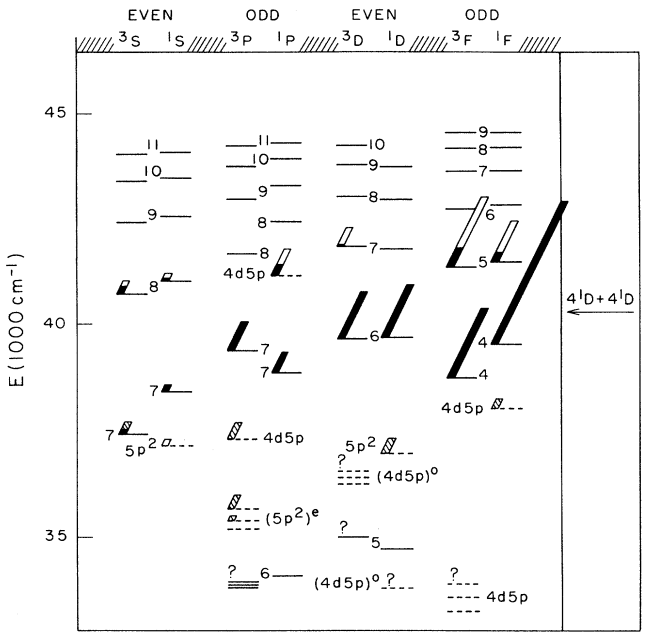

FIG. 7. The same as Fig. 5 for $4\,^1D+4\,^1D$ energy pooling.

cy is not as obvious from the results for $5\,^1P+5\,^1P$ energy pooling, although there also the largest rate coefficient is observed for an F state.

Total rate coefficients for EP to all states are given at the bottom of Tables II and III. When calculating this sum of the observed rate coefficients for $5\,^1P+5\,^1P$ energy pooling, we incorporate the values in column 8 of Table II for the ^{1,3}F levels, since for these levels the cascade contribution is mainly due to the population of higher angular momentum states, which should be included. In the case of $4\,^1D+4\,^1D$ energy pooling only data in the last column of Table III for energy levels above 37 000 cm^{-1} have been taken into account in the summation, since the rate coefficients of the lower energy levels are very likely to be heavily affected by cascade from levels which already have been included. For instance, a time-dependent measurement of the strong $5\,^1D\rightarrow 5\,^1P$ fluorescence at 7673 Å shows too slow a build in of the signal for direct energy pooling, and no quadratic dependence on the $4\,^1D$ density. This confirms our belief that the $5\,^1D$ level is predominately populated by cascade, although the estimate of the cascade contribution in column 9 of Table II is only $\sim 50\%$ of the uncorrected rate coefficient in column 8. The total rate coefficients, $(3.5\pm 1.3)\times 10^{-10}$ cm^3/s and $(2.1\pm 0.9)\times 10^{-10}$ cm^3/s in the case of $5\,^1P+5\,^1P$ and $4\,^1D+4\,^1D$ energy pooling, respectively, are on the order of the gas-kinetic rates, i.e., the probability of energy transfer per collision is high. (Since the fluorescence from certain levels is not detected in our experiment, this result of summing all measured rate coefficients is probably slightly smaller than the total rate coefficient for emptying the initial state.) This is not very surprising because of the high number of avoided crossings expected in this energy region where many molecular states occur, and the large statistical weight of the many final states which are energetically available.

ACKNOWLEDGMENTS

The authors gratefully acknowledge C. H. Greene and C. E. Theodosiou for calculating numerous Sr oscillator strengths, without which a meaningful analysis of our data would not have been possible, and D. A. Atkins for his assistance in the experiments. This work was supported in part by National Science Foundation Grant No. PHY86-04504.

*Present address: Van der Waals–Laboratorium, Universiteit van Amsterdam, Valckenierstraat 67, 1018 XE Amsterdam, The Netherlands.

†Present address: Royal Signals and Radar Establishment, Malvern, Worcestershire WR14 3PS, England.

‡Also at Department of Physics, University of Colorado, Boulder, CO 80309-0440.

§Also at Quantum Physics Division, National Institute of Stan-

dards and Technology, Boulder, CO 80309-0440.
[1]M. S. Child, *Molecular Collision Theory* (Academic, New York, 1974).
[2]M. Allegrini, G. Alzetta, A. Kopystynska, and L. Moi, Opt. Commun. **19**, 96 (1976).
[3]M. Allegrini, G. Alzetta, A. Kopystynska, L. Moi, and G. Orriols, Opt. Commun. **22**, 329 (1977).
[4]J. Huennekens and A. Gallagher, Phys. Rev. A **27**, 771 (1983).
[5]M. Allegrini, P. Bicchi, and L. Moi, Phys. Rev. A **28**, 1338 (1983).
[6]S. A. Davidson, J. F. Kelly, and A. Gallagher, Phys. Rev. A **33**, 3756 (1986).
[7]J. C. Kircz, R. Morgenstern, and G. Nienhuis, Phys. Rev. Lett. **48**, 610 (1982).
[8]H. R. Thorsheim, Y. Wang, and J. Weiner, Phys. Rev. A **41**, 2873 (1990). See reference herein.
[9]J. F. Kelly, M. Harris, and A. Gallagher, Phys. Rev. A **38**, 1225 (1988).
[10]S. Gozzini, S. A. Abdullah, M. Allegrini, A. Cremoncini, and L. Moi, Opt. Commun. **63**, 97 (1987).
[11]C. Gabbanini, S. Gozzini, G. Squadrito, M. Allegrini, and L. Moi, Phys. Rev. A **39**, 6148 (1989).
[12]E. N. Borisov, N. P. Perkin, and T. P. Redko, Opt. Spektrosk. **59**, 707 (1985) [Opt. Spectrosc. (USSR) **59**, 426 (1985)].
[13]J. F. Kelly, M. Harris, and A. Gallagher, Phys. Rev. A **37**, 2354 (1988).
[14]M. Harris, J. F. Kelly, and A. Gallagher, Phys. Rev. A **36**, 1512 (1987).
[15]I. Sakai, H. Ishimaru, and G. Horikoshi, Vacuum **32**, 33 (1982).
[16]H. G. C. Werij, C. H. Greene, and C. E. Theodosiou (unpublished).
[17]D. R. Bates and A. Damgaard, Philos. Trans. R. Soc. London, Ser. A **242**, 101 (1949).
[18]J. Huennekens and A. Gallagher, Phys. Rev. A **28**, 1276 (1983).
[19]T. Holstein, Phys. Rev. A **72**, 1212 (1947); **83**, 1159 (1951).
[20]C. van Trigt, Phys. Rev. A **181**, 97 (1969).
[21]A. L. Osherovich, Ya. F. Verolainen, S. A. Pulkin, V. I. Privalov, and S. M. Lupekhin, Opt. Spektrosk. **46**, 243 (1979) [Opt. Spectrosc. (USSR) **46**, 134 (1979)].
[22]U. Brinkmann, Z. Phys. **228**, 440 (1969).
[23]W. Gornik, Z. Phys. A **283**, 231 (1977).
[24]G. Jönsson, C. Levinson, A. Persson, and C.-G. Wahlström, Z. Phys. A **316**, 255 (1984).
[25]H. J. Andrä, H.-J. Plöhn, W. Wittmann, A. Gaupp, J. O. Stoner, and M. Gaillard, J. Opt. Soc. Am. **65**, 1410 (1975).
[26]N. M. Erdevdi and L. L. Shimon, Opt. Spektrosk. **40**, 771 (1976) [Opt. Spectrosc. (USSR) **40**, 443 (1976)].
[27]P. Grafström, Jiang Zhan-Kui, G. Jönsson, C. Levinson, H. Lundberg, and S. Svanberg, Phys. Rev. A **27**, 947 (1983).
[28]M. O. Hale and S. R. Leone, J. Chem. Phys. **79**, 3352 (1983).
[29]R. W. Schwenz and S. R. Leone, Chem. Phys. Lett. **133**, 433 (1987).
[30]W. H. Breckenridge and C. N. Merrow, J. Chem. Phys. **88**, 2329 (1988).
[31]W. H. Breckenridge and C. N. Merrow, J. Chem. Phys. **88**, 2320 (1988).
[32]J. F. Kelly, M. Harris, J. Cooper, and A. Gallagher, in *Abstracts of the Sixteenth International Conference on the Physics of Electronic and Atomic Collisions, New York, 1989,* edited by A. Dalgarno, R. S. Freund, M. S. Lubell, and T. B. Lucatorto (AIP, New York, 1990), p. 87.